T. Fröhlich, M. Hohmann, M. Schalles

Technische Universität Ilmenau, Institute for Process Measurement and Sensor Technology, POB 100565, 98684 Ilmenau

CALIBRATION BENCH FOR HEAT FLUX SENSORS

A new calibration bench was developed at the Institute for Process Measurement and Sensor Technology of Technische Universität Ilmenau to calibrate heat flux sensors (HFS). The bench provides well known temperatures at both sides of the HFS, from which the heat flux can be determined. The temperatures are determined using a method known from the calibration of contact surface thermometers. By means of the values measured by thermocouples distributed along the central axis of two homogenization blocks, the surface temperatures of each homogenization block, and thereby the surface temperatures of the HFS, are extrapolated. The extrapolated surface temperatures are controlled in a manner that the difference between the two temperatures changes in the range of 0 mK to 200 mK. Using these temperature differences and the sensor signal, the offset and the sensitivity of the HFS can be determined. HFS based on thermopiles and HFS based on the transversal seebeck-effect were constructed calibrated at the bench.

Key words: heat flux sensor, calibration, surface temperature

Introduction

Heat flux sensors (HFS) for heat flux of conductive origin are usually calibrated at calibration benches using the guarded-hot-plate-method [1]. This method requires a known heat flux through the sensor under test. This heat flux is usually provided by a heater on one side of the HFS, measured by means of the temperature difference over a plate with known geometry and thermal conductivity and dissipated in a heat sink on the other side of the HFS. One of the main requirements for this method is a one-directional heat flux from the heat source to and through the sensor under test, which can only imperfectly be provided. The calibration bench presented in this paper uses a different approach. It uses the determination of the surface temperature of the sensor under test to investigate its characteristics.

Design and operating principle

Calibration bench

The calibration bench is an axial symmetrical construction consisting of two meander-shaped heaters and two cylindrical homogenization blocks (steel 1.4301) with integrated thermocouples (TCs) type K, surrounded by an insulation made of alkaline-earth silicate wool (Fig. 1). The homogenization blocks are 76 mm in diameter and 25 mm in height. The geometry of the air gap between the blocks depends on the geometry of the sensor under test (the HFS). The power of the heaters on top of the upper and at the bottom of the lower homogenization block can be controlled individually and heat the bench in a temperature range from 20 °C to 400 °C.

The three TCs in each homogenization block are used to extrapolate to the blocks surface temperature using a quadratic polynomial approach. This method is known from the calibration of contact surface thermometers [2]. Using this method, the surface temperatures of the homogenization blocks and of the HFS respectively, are determined and used as controlled variable. By means of the heaters, the temperatures are controlled in a manner that the difference of the extrapolated surface temperatures changes from $\Delta T = 0$ K to $\Delta T = \pm 200$ mK. The temperature difference of 200 mK was found to be great enough to get an evaluable signal and small enough to get a not to high deformation of the thermal field.

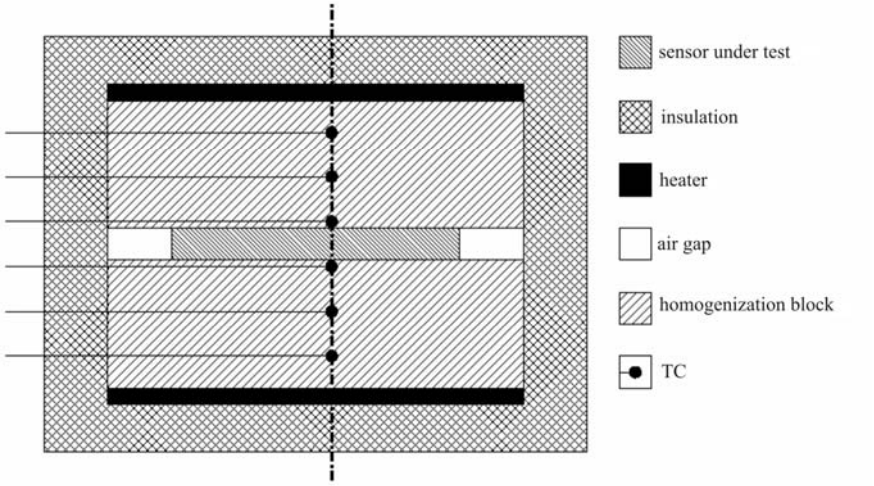

Fig. 1. Design of the calibration bench.

Operating principle

The aim of the calibration is to determine the sensitivity S and the offset U_0 of the characteristic (1) of the HFS, where ΔT is the temperature difference between top and bottom of the HFS.

$$U_{\mathrm{HFS}} = U_0 + S \cdot \Delta T \tag{1}$$

Each of the temperatures has errors due to temperature measurement and the unknown temperature field across the surface of the HFS (2).

$$U_{\mathrm{HFS}} = U_0 + S \cdot [(T_{\mathrm{upper}} + E_{\mathrm{upper}}) - (T_{\mathrm{lower}} + E_{\mathrm{lower}})] \tag{2}$$

To compensate the influence of these errors, two different temperature differences T_{upper}-T_{lower} (a and b) are used to determine $S(\Delta T)$. Assuming that the errors E are constant or change negligibly, $S(\Delta T)$ can be determined using the two signals U and the four temperatures T (3).

$$\begin{aligned} U_{\mathrm{HFS,a}} &= U_0 + S \cdot [(T_{\mathrm{upper,a}} + E_{\mathrm{upper}}) - (T_{\mathrm{lower,a}} + E_{\mathrm{lower}})] \\ U_{\mathrm{HFS,b}} &= U_0 + S \cdot [(T_{\mathrm{upper,b}} + E_{\mathrm{upper}}) - (T_{\mathrm{lower,b}} + E_{\mathrm{lower}})] \\ S(\Delta T) &= \frac{U_{\mathrm{HFS,a}} - U_{\mathrm{HFS,b}}}{(T_{\mathrm{upper,a}} - T_{\mathrm{lower,a}}) - (T_{\mathrm{upper,b}} - T_{\mathrm{lower,b}})} \end{aligned} \tag{3}$$

To determine the offset U_0, the HFS has to be flipped at one temperature or the polarity of the electrical connection to the measuring device has to be reversed (4).

$$U_{\mathrm{HFS,plus}} = U_0 + S \cdot [(T_{\mathrm{upper}} + E_{\mathrm{upper}}) - (T_{\mathrm{lower}} + E_{\mathrm{lower}})]$$
$$U_{\mathrm{HFS,minus}} = U_0 + S \cdot [(T_{\mathrm{lower}} + E_{\mathrm{lower}}) - (T_{\mathrm{upper}} + E_{\mathrm{upper}})] \quad (4)$$
$$U_0 = \frac{U_{\mathrm{HFS,plus}} + U_{\mathrm{HFS,minus}}}{2}$$

To get the sensitivity as a function of heat flux $\dot{q}$, the one-dimensional formulation of Fourier's law (5) is used, where λ is the thermal conductivity. With the assumptions of one-dimensional heat conduction and a constant temperature gradient across the length *l* of the sensor one gets (6).

$$\dot{q} = -\lambda \nabla T \quad (5)$$

$$\dot{q} = -\frac{\lambda}{l} \Delta T \quad (6)$$

Using equations (3) and (6), the sensitivity $S(\dot{q})$ is given by equation (7). The thermal conductivity and the thickness are temperature-dependent, but their changes in the small temperature interval of 200 mK can be neglected.

$$S(\dot{q}) = \frac{l}{\lambda} \cdot \frac{U_{\mathrm{HFS,a}} - U_{\mathrm{HFS,b}}}{(T_{\mathrm{upper,a}} - T_{\mathrm{lower,a}}) - (T_{\mathrm{upper,b}} - T_{\mathrm{lower,b}})} \quad (7)$$

Sensors under test

The sensors under test were constructed at the Institute for Process Measurement and Sensor Technology of the Technische Universität Ilmenau. Two principles were used: one design using thermopiles, which is a well-known principle for HFS [3], and one design using the transversal seebeck-effect [4], [5]. Both types of sensors were constructed with the same geometrical parameters, disks with 54 mm in diameter and 1.5 mm in height.

HFS using thermopiles

The sensors consist of two rings of TCs type E, which are thermally connected in parallel and electrically connected in series. These so called thermopiles have 25 junctions at the inner and 35 junctions at the outer ring and are mounted to a backing made of glass ceramic (λ = 1.72 W m^{-1} K^{-1}, Fig. 2). To investigate the influence of the filling (heat conducting compound, λ = 3 W m^{-1} K^{-1}), sensors with and without filling were constructed.

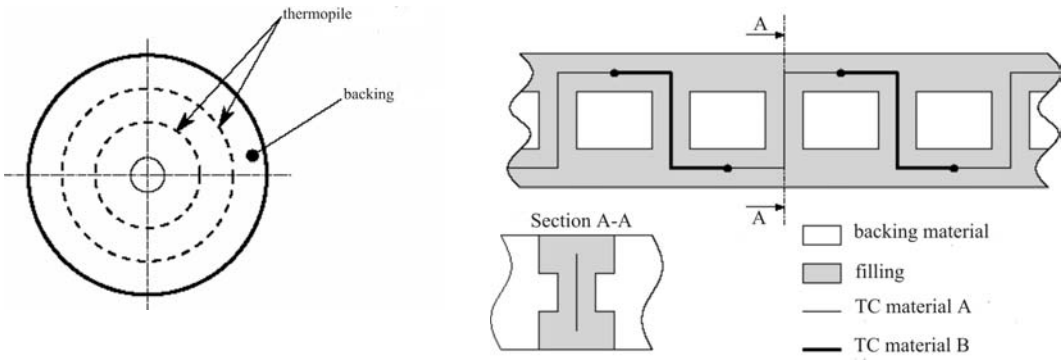

Fig. 2. Design of the HFS and cross-section along one thermopile.

The theoretical sensitivity $S(\dot{q})$ (8) depends on the sensitivity $S_{\mathrm{TC}}(T)$ of the TC type E, the distance between the junctions l_{J}, the thermal conductivity and the number n of TCs in the thermopile [3]. The sensitivity $S(\Delta T)$ only depends on $S_{\grave{O}\tilde{N}}(T)$ and n (9).

$$S(\dot{q}) = \frac{n \cdot S_{\mathrm{TC}}(T) \cdot l_{\mathrm{J}}}{\lambda} \tag{8}$$

$$S(\Delta T) = n \cdot S_{\mathrm{TC}}(T) \tag{9}$$

To estimate the theoretical sensitivity, the equivalent electrical circuit [2] was used. With this model and the values for $S_{\mathrm{TC}}(T)$ from [6] for different temperatures the sensitivity was estimated (Table 1).

Table 1

Theoretical sensitivity of the HFS using thermopiles.

	60 °C		100 °C		150 °C	
thermopile	$S(\Delta T)$, μVK^{-1}	$S(\dot{q})$, $\mu VW^{-1}m^2$	$S(\Delta T)$, μVK^{-1}	$S(\Delta T)$, μVK^{-1}	$S(\dot{q})$, $\mu VW^{-1}m^2$	$S(\Delta T)$, μVK^{-1}
25 with filling	56.96	406.83	58.61	56.96	406.83	58.61
35 with filling	79.66	568.28	81.96	79.66	568.28	81.96
25 without filling	40.42	194.97	41.59	40.42	194.97	41.59
35 without filling	56.51	272.20	58.14	56.51	272.20	58.14

HFS using transversal Seebeck-effect

The sensors main part is a solid disk made of a stack of *NiCr*- and *CuNi*-layers. These metals (material for TC-type E) are welded by means of diffusion welding and cut into disks under an angle of 45° (Fig. 3). In this artificial anisotropic material, the Seebeck coefficient σ and the thermal conductivity λ are tensors of second order and described by (10) and (11), where $\lambda_{\parallel}$ and $\sigma_{\parallel}$ represent the material properties along, $\lambda_{\perp}$ and $\sigma_{\perp}$ the properties perpendicular to the main axis of the stack [5].

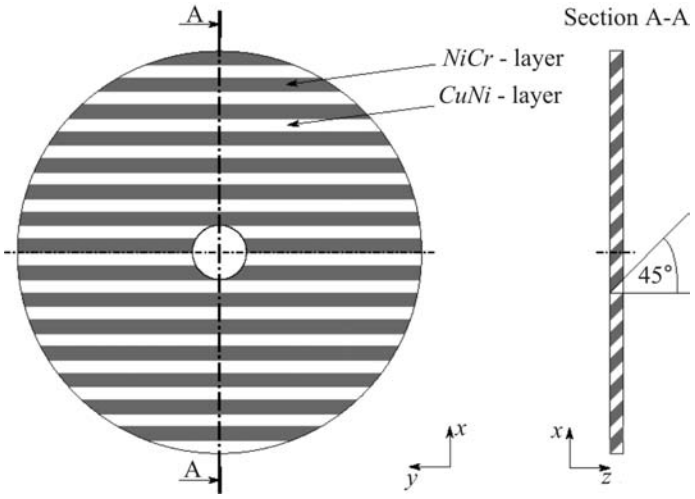

Fig. 3. Design of the HFS made of artificial anisotropic material.

$$\sigma = \begin{bmatrix} \sigma_P \cos^2\alpha + \sigma_\wedge \sin^2\alpha & 0 & \frac{1}{2}(\sigma_P - \sigma_\wedge)\sin(2\alpha) \\ 0 & \sigma_P & 0 \\ \frac{1}{2}(\sigma_P - \sigma_\wedge)\sin(2\alpha) & 0 & \sigma_P \cos^2\alpha + \sigma_\wedge \sin^2\alpha \end{bmatrix} \tag{10}$$

$$\lambda = \begin{bmatrix} \lambda_\square \cos^2\alpha + \lambda_\perp \sin^2\alpha & 0 & \frac{1}{2}(\lambda_\square - \lambda_\perp)\sin(2\alpha) \\ 0 & \lambda_\square & 0 \\ \frac{1}{2}(\lambda_\square - \lambda_\perp)\sin(2\alpha) & 0 & \lambda_\square \cos^2\alpha + \lambda_\perp \sin^2\alpha \end{bmatrix} \tag{11}$$

The signal of the sensor is the electric field E generated by the thermopower inside the sensor (12) integrated along the direction of the measured voltage, x in this case (13).

$$E = \sigma \cdot \nabla T \tag{12}$$

$$U_x = \int_0^d \left(\left(\sigma_\square \cos^2\alpha + \sigma_\perp \sin^2\alpha\right)\frac{\partial T}{\partial x} + \frac{1}{2}\left(\sigma_\square - \sigma_\perp\right)\sin(2\alpha)\frac{\partial T}{\partial z} \right) dx \tag{13}$$

Assuming one-dimensional heat conduction in z-direction with a constant gradient, one gets the sensor signal as a function of the temperature difference ΔT in *z*-direction (14).

$$U_x = \frac{1}{2}\left(\sigma_\square - \sigma_\perp\right)\sin(2\alpha)\frac{d}{l}\Delta T_z \tag{14}$$

Hence, the theoretical sensitivity $S(\Delta T)$ depends on the anisotropy of the thermopower $\left(\sigma_\square - \sigma_\perp\right)$, the cutting angle α, the diameter *d* and the thickness *l* of the sensor. The theoretical sensitivity $S(\dot{q})$ additionally depends on the thermal conductivity λ in *z*-direction.

$$S(\Delta T) = \frac{U_x}{\Delta T_z} = \frac{1}{2}\left(\sigma_\square - \sigma_\perp\right)\sin(2\alpha)\frac{d}{l} \tag{15}$$

$$S(\dot{q}) = \frac{U_x}{\dot{q}_z} = \frac{\left(\sigma_\square - \sigma_\perp\right)\sin(2\alpha)d}{\left(\lambda_\square \cos^2\alpha + \lambda_\perp \sin^2\alpha\right)l} \tag{16}$$

Differently from the HFS using thermopiles, the theoretical sensitivity of this design depends on more material properties. In addition to the ones already mentioned, the electrical resistivity is used to determine $\sigma_\square$ [5]. Since these material properties are not exactly known and several different values can be found in references, a Monte-Carlo simulation of the sensitivity was carried out using the values listed in Table 2 and a variation of $\pm 20\,\%$ for each of them.

Table 2

Material properties of NiCr and CuNi [2], [7], [8], [9].

material	σ, μVK^{-1}	λ, $Wm^{-1}K^{-1}$	γ, $\mu\Omega^{-1}m^{-1}$
NiCr	28.07	19.0	1.4
CuNi	-42.05	25.29	2.0

The results of this simulation are minimal and maximal expected values for the sensitivity at the three temperatures, which are shown in Table 3. The high difference of the minimal and maximal expected values can be explained by the nonlinear relation of the material properties in the model (10). The calculated values define a range, in which the calibration results should be lying to be considered as valid.

Table 3

Minimal and maximal theoretical sensitivity of the HFS using transversal Seebeck effect.

	60 °C		100 °C		150 °C	
value	$S(\Delta T)$, μVK^{-1}	$S(\dot{q})$, $nVW^{-1}m^2$	$S(\Delta T)$, μVK^{-1}	$S(\dot{q})$, $nVW^{-1}m^2$	$S(\Delta T)$, μVK^{-1}	$S(\dot{q})$, $nVW^{-1}m^2$
minimum	0.46	0.06	0.52	0.07	0.56	0.08
maximum	421.80	59.89	441.74	62.83	467.90	66.44

Properties of the bench

Stability of the surface temperatures

Each of the extrapolated surface temperatures is controlled by a PID-controller respectively. These controllers are able to hold the setpoint, but there are oscillations with a period of about 300 s and a magnitude less than 30 mK around the setpoint (Fig. 4). These oscillations are caused by the periodic change of the temperature in the laboratory due to air condition, cross-sensitivity of the two controllers and the nonexistent active cooling. Nevertheless this quality of the controlled temperatures is sufficient for calibration, since integration intervals of 600 s are possible during the calibration process.

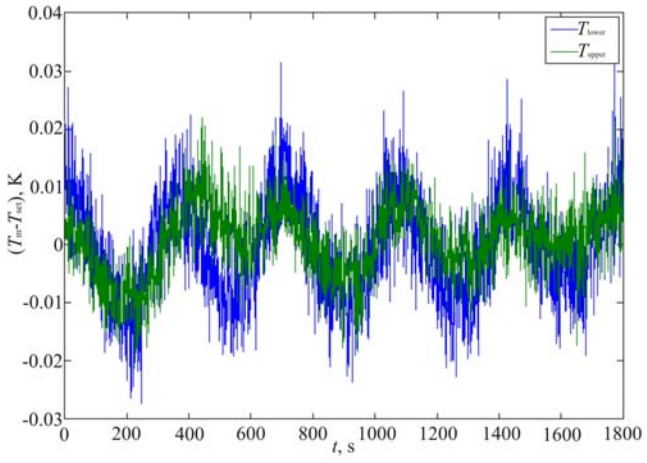

Fig. 4. Temperature differences between the setpoint temperature T_{set} and the measured surface temperatures T_m of the upper and the lower homogenization block in steady state.

Axial temperature distribution

Fig. 5 shows the axial temperature distribution in the blocks during the calibration at $T_{set} \sim 100$ °C with a temperature difference of T_{upper}-$T_{lower} = 100$ mK. In each block the temperature distribution follows a quadratic function. The deviation of a linear distribution is caused by the heat exchange with

the other block respectively and the heat losses through the non-ideal insulation. The temperature distribution across both blocks is an indication of the influence of thermal contact resistances between the HFS and the blocks surfaces.

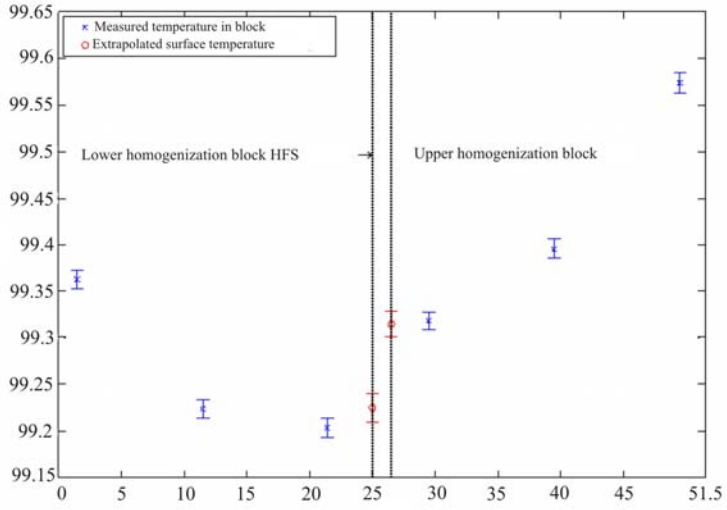

Fig. 5: Axial temperature distribution from height h=0 mm (bottom) to h=51.5 mm (top) of the bench at T_{set} ~ 100 °C and the temperature difference T_{upper}-T_{lower} = 100 mK. The error bars show the standard deviation of the temperatures (2500 data points).

Homogeneity of the temperature field

To estimate the homogeneity of the temperature field across both sides of the HFS, a TC was used to measure the surface temperatures at several points. For this, a dummy of a HFS with a radial groove was manufactured in which the TC was inserted. For each measurement series, the dummy was rotated 45°. At every angular step, the TC was moved in the groove from the center outwards in 2.5 mm-steps. This measurement was performed at steady state of the surface temperatures at 60 °C. The results in show, that the absolute temperature difference across the each surface has a magnitude of 160 mK.

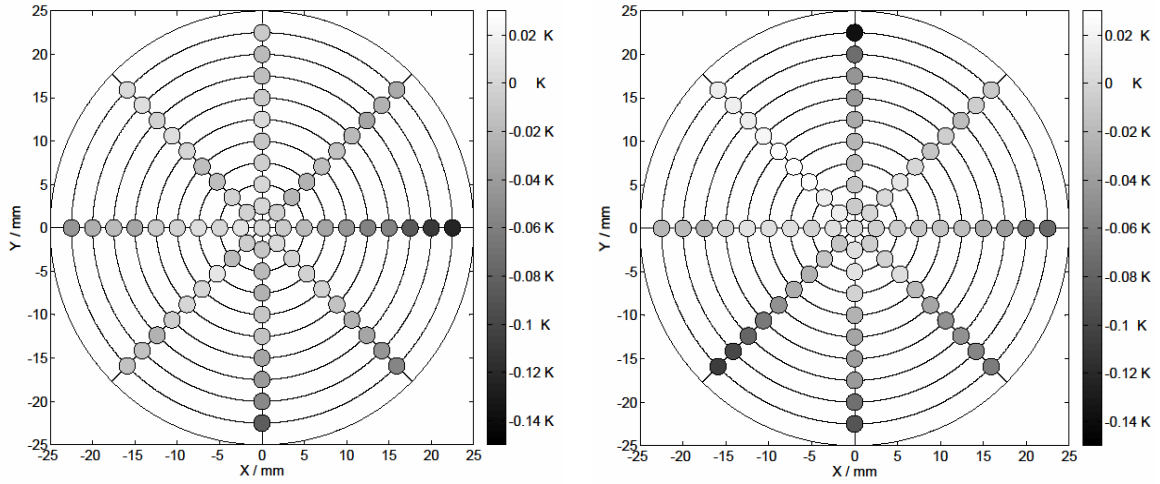

a) *b)*

Fig. 6. Temperature field at the surface of the upper (a) and the lower (b) homogenization block at T_{set} = 60 °C, the difference to the extrapolated surface temperature at the center is shown.

The difference of the measured temperature field compared to a typical one with gradient in radial direction can be explained by the shape of the heaters. Due to the non-uniform heat input, the temperature field gets deformed, which has been simulated with the Finite Element Method (Fig. 7).

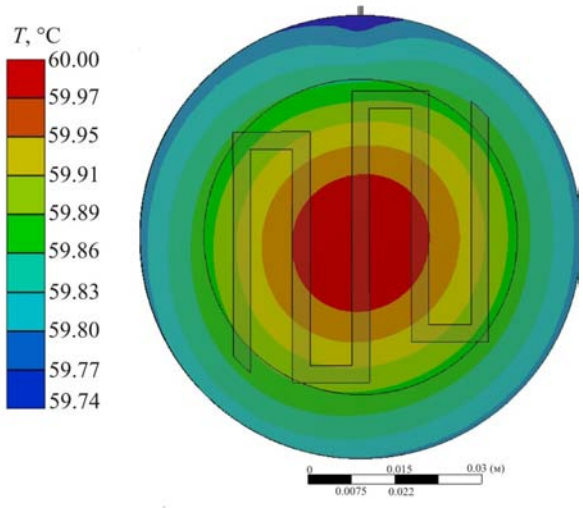

Fig. 7. FEM-Simulation of the temperature field due to the non-uniform heat input. The homogenization block, the heater and the position of the HFS are shown.

Calibration results

HFS using thermopiles

Due to the long integration interval at every calibration point, the calibration at one temperature takes about 5 h. During this time, 5 calibration points are measured (Figr. 8, Fig. 9). To determine the sensitivity, these points are taken to fit a polynomial of first degree in a least-squares-manner, which fulfills equation (3). The offset results from temperature differences due to the calibration of the TC inside the normalization blocks.

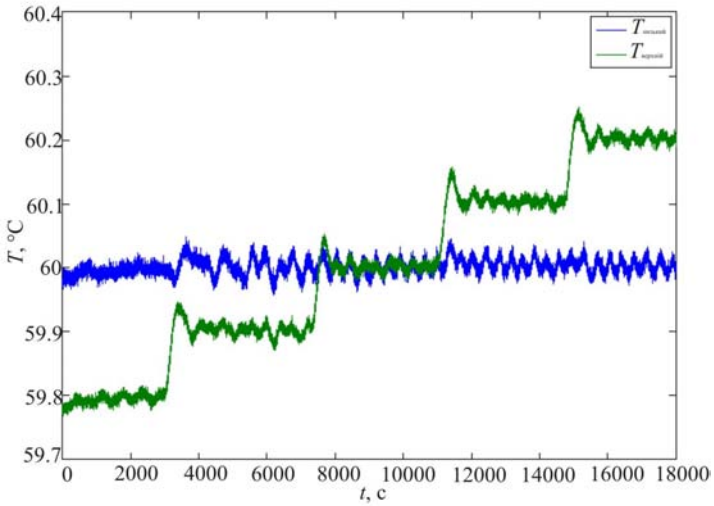

Figr. 8. Temperatures during the calibration around 60 °C.

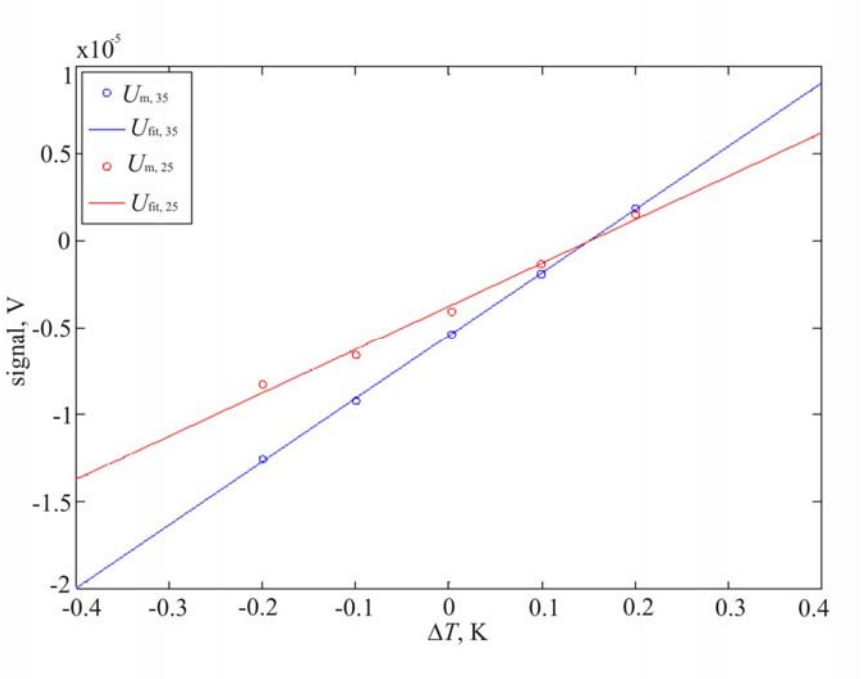

Fig. 9. Sensor signals during the calibration around 60 °C. U_m is the measured signal of each thermopile, U_{fit} is the approximated polynomial of first grade from which the sensitivity is taken.

The high differences between the theoretical values and the measured ones (Table 4) are caused by the thermal resistances between the HFS and the blocks surfaces. These resistances can hardly be measured, but are also present at the real application. Due to this, the measured sensitivities can be used in the application if the surface properties and the contact forces are comparable to the calibration circumstances.

Table 4

Measured sensitivity of the HFS using thermopiles.

	60 °C		100 °C		150 °C	
thermopile	$S(\Delta T)$, μVK^{-1}	$S(\dot{q})$, $\mu VW^{-1}m^2$	$S(\Delta T)$, μVK^{-1}	$S(\dot{q})$, $\mu VW^{-1}m^2$	$S(\Delta T)$, μVK^{-1}	$S(\dot{q})$, $\mu VW^{-1}m^2$
25 with filling	25.52	182.27	28.56	203.95	29.91	213.59
35 with filling	36.63	261.31	36.64	261.37	38.66	275.80
25 without filling	27.19	131.15	30.22	145.75	32.34	155.98
35 without filling	41.14	198.17	46.60	224.43	50.31	242.31

The relative error E_r (17) of the measured sensitivity S_m to the theoretical S_t (Table 5) shows, that the relative error gets smaller with higher temperature and if there is no filling in the HFS. This indicates the influence of the contact resistance. These contact resistances have a higher influence on the sensitivity than the heat conduction trough air or ceramic filler. Additionally, the influence of heat transfer by radiation becomes greater at higher temperatures when there is only air between the thermopiles and the surface of the homogenization blocks.

$$E_r = \frac{S_m - S_t}{S_t} \cdot 100 \qquad (17)$$

Table 5

Relative error of the sensitivity.

	60 °C	100 °C	150 °C
thermopile	E_r / %	E_r / %	E_r / %
25 with filling	-55.20	-51.27	-50.59
35 with filling	-54.02	-55.30	-54.32
25 without filling	-32.73	-27.34	-24.70
35 without filling	-27.20	-19.85	-16.22

HFS using transversal Seebeck effect

The same temperature sequence as shown in Figr. 8 was used for this calibration. The results also show an offset due to the calibration of the TC inside the normalization blocks. The measured values for the sensitivity are shown in Table 6, where the material properties of Table 2 were used to calculate $S(\dot{q})$. The values are in the expected range and an increasing sensitivity with increasing absolute temperature can be seen.

Table 6

Measured sensitivity of the HFS using transversal Seebeck effect.

60 °C		100 °C		150 °C	
$S(\Delta T)$ / μVK^{-1}	$S(\dot{q})$ / $nVW^{-1}m^2$	$S(\Delta T)$ / μVK^{-1}	$S(\Delta T)$ / μVK^{-1}	$S(\dot{q})$ / $nVW^{-1}m^2$	$S(\Delta T)$ / μVK^{-1}
4.93	0.68	5.50	0.75	6.09	0.83

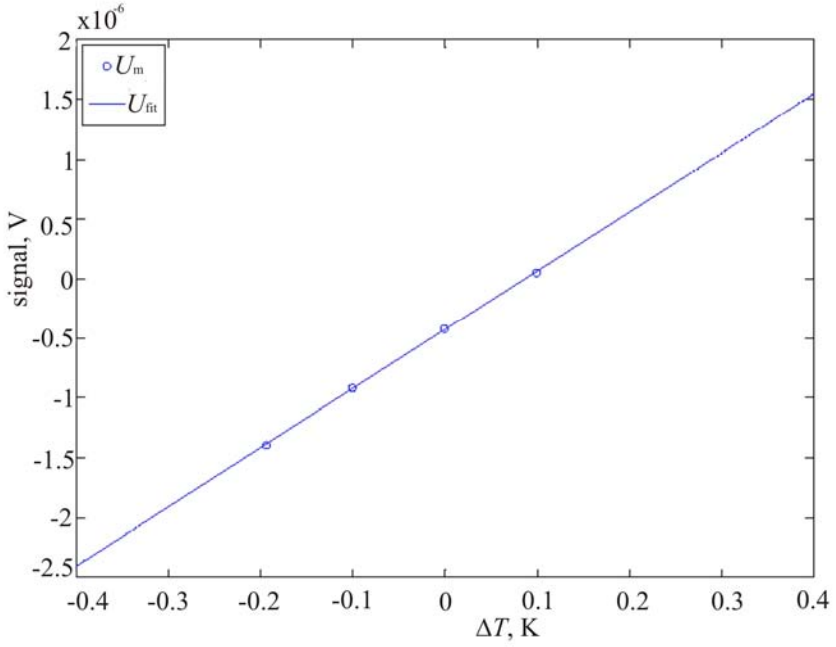

Fig. 10: Sensor signals during the calibration around 60 °C. U_m is the measured signal, U_{fit} is the approximated polynomial of first grade from which the sensitivity is taken.

Conclusion and outlook

A new bench for the calibration of heat flux sensors was developed, built up and tested. The thermal properties of the bench like stability of the temperature and axial and radial temperature distribution were measured. The results show, that the bench can be used to calibrate HFS with small heat fluxes. Two types of sensors were calibrated, the measured sensitivities compared to the theoretical ones show that every measurement with a HFS has to be checked carefully due to thermal contact resistances. A first set of calibrations from 60 °C to 150 °C has already been carried out, the test with temperatures up to 400 °C is in progress.

Acknowledgement. The authors would like to thank the German Federal Ministry of Education and Research (BMBF) for the financial support of the VIP-Project “TempKal”, in which context this calibration bench was developed.

References

1. F.Arpino, M.Dell’Isola, G.Ficco, L.Iacomini, V.Fernicola, Design of a Calibration System for Heat Flux Meters, International Journal of Thermophysics **32**(11-12), 2727-2734 (2011).
2. F.Bernhard (Ed.), Technische Temperaturmessung (Berlin: Springer-Verlag, 2004).
3. P.R.N.Childs, J.R.Greenwood, C.A.Long, Heat Flux Measurement Techniques. In: Proceedings of the Institution of Mechanical Engineers, Part C: Journal of Mechanical Engineering Science (1999), p. 655-677
4. Andrey V.Mityakov, Sergey Z.Sapozhnikov, Vladimir Y.Mityakov, Andrei A.Snarskii, Maxim I.Zhenirovsky, Juha J.Pyrhönen, Gradient Heat Flux Sensors for High Temperature Environments, Sensors and Actuators A: Physical **176**,1-9 (2012).
5. K.Fischer, C.Stoiber, A. Kyarad, H.Lengfellner, Anisotropic Thermopower in Tilted Metallic Multilayer Structures, Applied Physics A: Materials Science & Processing **78,** 323-326 (2004).
6. DIN EN 60584-1: Thermopaare. Teil 1: Grundwerte der Thermospannung (1996)
7. ASTM, Standard Specification and Temperature-Electromotive Force (EMF) Tables for Standardized Thermocouples, 2003.
8. O.Madelung and G.K.White (Ed.): Landolt-Börnstein, Zahlenwerte und Funktionen aus Naturwissenschaften und Technik: Gruppe III: Kristall- und Festkörperphysik. Bd. 15: Metalle: Elektronische Transportphänomene, Teilband c: Wärmeleitfähigkeit von reinen Metallen und Legierungen (Berlin Heidelberg New York Paris Tokyo Hong Kong Barcelona Budapest: Springer, 1991).
9. J.R.Davis, Heat-Resistant Materials, ASM Specialty Handbook (Materials Park Ohio: ASM International, 1997).

Submitted 19.02.2015